Arch Biol Sci. 2024;76(4):465-476 https://doi.org/10.2298/ABS240928036C

Inhibiting METTL3-ATG5 axis-mediated harmful autophagy in macrophages could help reduce airway epithelial inflammation and remodeling in COPD

Guiyang Chen[1], Zhiwei Xia[2], Xianyou Zeng[1] and Hanying Liu[3,*]

[1]*Department of Cardiology, Hunan Aerospace Hospital, No.189*, Fenglin 3rd Road, Changsha, 410205, China

[2]*Department of Neurology, Hunan Aerospace Hospital, No.189*, Fenglin 3rd Road, Changsha, 410205, China

[3]*Health Management Medicine Center, the Third Xiangya Hospital, Central South University*, 138 Tongzipo Road, Changsha, 410013, China

***Corresponding author**: liuduolin@csu.edu.cn

Received: September 28, 2024; **Revised**: October 29, 2024; **Accepted**: October 31, 2024; **Published online**: November 7, 2024

Abstract: Cigarette smoke exposure leads to chronic obstructive pulmonary disease (COPD). We investigated the role and underlying mechanisms of methyltransferase-like 3 (METTL3) and autophagy-related protein 5 (ATG5) in the progression of COPD. In a COPD mouse model exposed to cigarette smoke, lung tissues showed increased levels of METTL3, p-p65/p65, autophagy markers (LC3 and ATG5), inflammatory factors (interleukin-6, IL-8, and TNF-α), and airway remodeling markers (N-cadherin, α-SMA, and Tn-C), while p62 and E-cadherin levels were decreased. Expression of METTL3 and ATG5 was positively correlated. These findings are consistent with observations in RAW264.7 mouse mononuclear macrophages exposed to cigarette smoke extract (CSE). CSE inhibited cell viability while promoting autophagy. METTL3 knockdown counteracted CSE effects, and ATG5 overexpression reversed METTL3 knockdown outcomes. Methylated RNA immunoprecipitation-qPCR showed that METTL3 knockdown reduced m6A, and the actinomycin D assay suggested that METTL3 knockdown reduced ATG5 mRNA levels and lowered ATG5 mRNA stability. METTL3-knockdown RAW264.7 reduced the inflammation and airway remodeling markers in the co-cultured mouse bronchial epithelial cells. In conclusion, inhibition of the METTL3-ATG5 axis-mediated macrophage detrimental autophagy in COPD could alleviate bronchial epithelial cell inflammation and reduce airway remodeling.

Keywords: chronic obstructive pulmonary disease (COPD); methyltransferase-like 3 (METTL3); autophagy-related protein 5 (ATG5); damaging autophagy

Abbreviations: chronic obstructive pulmonary disease (COPD); cigarette smoke extract (CSE); autophagy-related proteins 5 (ATG5); N6-methyladenosine (m6A); methyltransferase-like 3 (METTL3); bronchoalveolar lavage (BAL); enzyme-linked immunosorbent assay (ELISA); small interfering (si); microtubule-associated proteins 1A/1B light chain 3B (LC3); reverse transcription-quantitative polymerase chain reaction (RT-qPCR); cell counting kit-8 (CCK-8); optical density (OD); methylated RNA immunoprecipitation (MeRIP); standard deviation (SD); analysis of variance (ANOVA)

INTRODUCTION

Chronic obstructive pulmonary disease (COPD), which is currently the fourth most common cause of mortality worldwide, is a serious global health concern [1]. COPD patients exhibit sustained airflow limitation and respiratory symptoms [2]. Research has shown that macrophage-damaging autophagy is directly related to lung pathogen infection, airway inflammation, cell apoptosis, oxidative stress, emphysema, and other processes [3]. Macrophage-damaging autophagy affects the progression of COPD by influencing its polarization, the release of inflammatory factors, phagocytic clearance, and antigen presentation capacity [4,5]. A thorough examination of the role and mechanism of macrophage-damaging autophagy in the progression of COPD is crucial for effective disease mitigation.

Cigarette smoke exposure is the most important factor leading to COPD [6]. Studies have shown that cigarette smoke extract (CSE) impairs the autophagic degradation process, leading to increased

macrophage-damaging autophagy, with elevated levels of autophagy-related proteins 5 (ATG5) observed [7,8]. Dysregulation of autophagy induced by cigarette smoke/CSE exposure leads to ciliary dysfunction and airway epithelial cell death, as well as induction of impaired autophagy and cellular senescence, thereby accelerating COPD progression [9,10]. ATG5 is a key molecule in the autophagy process. Research has shown that ATG5 plays an important role in regulating the autophagy process, helping to clear damaged proteins, organelles, and other cellular components, thus maintaining cellular health and the balance of the internal environment [11,12]. TNF in keratinocytes upregulates ATG5 levels while activating the NF-κB pathway, which is accompanied by fibroblast activation and inflammatory cell recruitment [13]. However, the relationship between macrophage-damaging autophagy and ATG5 in COPD is unclear. Exploring this relationship and its potential signaling pathways may help develop novel avenues for COPD treatment.

RNA methylation is a reversible epigenetic modification, with m6A being the most common type of mRNA methylation modification [14]. Studies have determined that m6A modification is crucial for regulating RNA splicing, transport, translation, and stability and is closely related to the occurrence and progression of various human diseases [15]. The m6A-modified circSAV1 promotes the translation of IREB2 by recruiting YTHDF1, thereby triggering ferroptosis in COPD [16]. METTL3-mediated m6A modification induces the degradation of the UBX protein domain 1, activation of NF-κB, and the malignant development of gliomas [17]. After exposure to 5% CSE, METTL3 mRNA levels significantly increase in human bronchial epithelial cells [18]. METTL3, a core component of the N6-methyladenosine (m6A) methyltransferase, has been shown to target ATG5 in germ cell malignancies to control autophagy and cisplatin sensitivity [19]. The mechanism of METTL3-ATG5 axis action in COPD has not been reported.

Based on the information above, we predict that the METTL3-ATG5 axis plays an important role in macrophage-damaging autophagy in COPD and influences bronchial epithelial inflammation and airway remodeling. We aimed to investigate the function and underlying mechanisms of action of the METTL3-ATG5 axis in COPD.

MATERIALS AND METHODS

Animal experiments

This study was approved by the Medical Ethics Committee of Hunan Aerospace Hospital (No. HNHTYY20230412LLSH-016-01). Male C57BL/6 mice (8 weeks, 20-25 g) were purchased from the Hunan Slake Jingda Animal Experimental Company. Based on previous studies, a COPD mouse model was established using the cigarette smoke exposure method [20]. In brief, the mice were housed at 22-24°C on a standard diet with a 12 h light-dark cycle. After adaptation for 1 week, 12 C57BL/6 mice were randomly divided into control and experimental model groups, with 6 mice in each group. Experimental mice were placed in a 33×25×23 cm exposure box. Cigarettes with a tar content of 11 mg, nicotine content of 1.1 mg, and CO content of 12 mg, (China Tobacco Chongqing Industrial Co., Ltd.) were lit, and the smoke was administered once daily (20 cigarettes each time) 5 times per week. Smoke exposure continued for 12 weeks [21]. The control group was maintained under normal air condition. At the end of the experiment, the mice were euthanized with pentobarbital sodium (200 mg/kg, intraperitoneal injection), and lung tissues were collected for further research. Bronchoalveolar lavage (BAL) was performed by opening the chest cavities of mice. Phosphate-buffered saline (PBS, 800 μL) was slowly injected into the lungs through the trachea, followed by a gentle withdrawal. BAL was performed 3 times, and lavage fluid was collected and centrifuged at 2000 ×*g* for 10 min. The cell-free supernatant was stored at -80°C for the enzyme-linked immunosorbent assay (ELISA).

Histological staining

After 12 h of baking at 60°C, the mouse lung tissue slices were dewaxed in water. Hematoxylin (AWI0001a, Abiowell, China) and eosin (AWI0001a, Abiowell) dyes were used to stain the sections for H&E staining. For Masson staining, the sections were stained with hematoxylin (60532ES58, Yeasen, China), lisianthus-acid magenta (60532ES58, Yeasen), and aniline blue (60532ES58, Yeasen). After staining, the slices were sealed, blow-dried, and examined under a light microscope (BA210T, Motic).

Cell culture

The mouse monocyte macrophage RAW264.7 (AW-CCM002, Abiowell) and mouse primary bronchial epithelial cells (MIC-iCell-a008, iCell Bioscience Inc. China) were cultured in Dulbecco's modified Eagle Medium (DMEM) (AW-MC001, Abiowell) containing 10% fetal bovine serum (AWC0219a, Gibco) and 1% penicillin/streptomycin (AWH0529a, Abiowell). The cells were incubated at 37°C with 5% CO_2 in a culture incubator. Cell COPD modeling: CSE at increasing concentrations (0, 1, 2.5, 5, or 10%) was applied to RAW264.7 cells for 48 h [22]. The smoke from 20 cigarettes was collected using a syringe and bubbled into 50-mL DMEM. After titration to pH 7.40±0.05 and sterilization with a 0.22-μm filter (FPE204030, Biofil, China), the DMEM containing cigarette components was regarded as 100% CSE. The CSE was diluted to specific concentrations with DMEM for subsequent cell treatment.

Cell transfection

Transfection was performed in RAW264.7 cells using lipofectamine 2000 (11668019, Invitrogen Thermo Fischer Scientific, China) according to the manufacturer's instructions [23]. The following oligos or plasmids were used for cell transfection: mice small interfering (si)-METTL3 (HG-SM019721, Honorgene, China), mice overexpression (oe)-ATG (HG-OM053069, Honorgene), and their blank controls si-NC and oe-NC. To screen out the most effective si-METTL3 from the three oligos provided by the manufacturer, si-METTL3#1, si-METTL3#2, and si-METTL3#3 were transfected into RAW264.7 cells, respectively. The one that led to the lowest expression of METTL3 was selected as the si-METTL3 for subsequent studies.

Experimental grouping

There were 10 groups in the cell experiments as follows: (i) the control group: RAW264.7 cells that were cultured normally; (ii) si-NC group: si-NC was used to transfect RAW264.7 cells; (iii) si-METTL3 group: si-METTL3 was used to transfect RAW264.7 cells; (iv) CSE+si-NC group: following 10% CSE intervention for 48 h, si-NC was transfected into RAW264.7 cells; (v) CSE+si-METTL3 group: following 10% CSE intervention for 48 h, si-METTL3 was transfected into RAW264.7 cells; (vi) CSE+si-METTL3+Rapa group: following 10% CSE intervention for 48 h, si-METTL3 was transfected into RAW264.7 cells, followed by treatment with 5 nM rapamycin (an autophagy inducer) or (AY22989, Sirolimus) for 24 h; (vii) oe-NC group: oe-NC was used to transfect RAW264.7 cells; (viii) oe-ATG5 group: oe-ATG5 was used to transfect RAW264.7 cells; (ix) CSE+si-METTL3+oe-NC group: following exposure to 10% CSE for 48 h, si-METTL3 and oe-NC were transfected into RAW264.7 cells; (x) CSE+si-METTL3+oe-ATG5 group: following 10% CSE intervention for 48 h, si-METTL3 and oe-ATG5 were transfected into RAW264.7 cells. The bronchial epithelial cell CSE, CSE+si-NC, CSE+si-METTL3, and CSE+si-METTL3+Rapa groups were co-cultured with matching RAW264.7 cells for 48h, respectively.

Western blotting

The cells and tissues of each group were collected and washed with pre-cooled PBS buffer, and radioimmunoprecipitation assay (RIPA) lysis buffer (AWB0136, Abiowell) was added to lyse the samples. About 25 mg of tissue was washed using PBS, and 300 μL RIPA lysis buffer was added; a biosample homogenizer (BioPrep-24, Allsheng) was used until the tissue block disappeared. For cell processing, 200 μL of RIPA lysis buffer was added to each well of a 6-well plate after washing the cells with PBS. The cells were then scraped from the plate and disrupted using an ultrasonic cell disruptor (XM-250T, Xiaomei) for 1.5 min. After determining the protein concentration in the lysate with a bicinchoninic acid kit (AWB0156, Abiowell), protein samples of equal volumes were combined with 5×loading buffer (AWB0055, Abiowell) and boiled in a water bath for 5 min to denature the proteins.

Electrophoresis was performed in a 10% polyacrylamide gel at a constant voltage of 75 V using a vertical electrophoresis apparatus (DYCZ-24DN, Liuyi) until the bromophenol blue trace of the loading buffer reached the bottom of the gel. The proteins in the gels were transferred to a nitrocellulose membrane (AWB0231a, Abiowell) at a constant current of 300 mA using a transfer apparatus (DYCZ-40D, Liuyi) [24]. The membrane was then rinsed once in 1×phosphate-buffered saline with Tween 20 (PBST) and completely immersed in the blocking solution. The membrane was shaken at room

temperature for 90 min. Primary antibodies METTL3 (15073-1-AP, 1:1000, Proteintech), light chain 3B (LC3B) (18725-1-AP, 1:500, Proteintech), ATG5 (10181-2-AP, 1:1000, Proteintech), p62 (18420-1-AP, 1:4000, Proteintech), p-p65 (AWA47471, 1:1000, Abiowell), p65 (AWA00848, 1:2000, Abiowell), N-cadherin (22018-1-AP, 1:5000, Proteintech), α-smooth muscle actin (α-SMA) (AWA46841, 1:1000, Abiowell), TN-C (67710-1-Ig, 1:5000, Proteintech), E-cadherin (20874-1-AP, 1:5000, Proteintech), and β-actin (66009-1-Ig, 1:5000, Proteintech) were diluted with 1×PBST. The membrane was left at room temperature for 30 min after incubating with primary antibodies overnight at 4°C. After incubation, the membranes were treated with the diluted secondary antibodies HRP goat anti-mouse IgG (SA00001-1, 1:5000, Proteintech) and HRP goat anti-rabbit IgG (SA00001-2, 1:6000, Proteintech) at room temperature for 90 min. To observe the blot bands, the membrane was incubated with the ECL chemiluminescence solution (AWB0005, Abiowell), and images of the membrane were captured using chemiluminescence imaging equipment (ChemiScope6100, Clinx Science Instruments). The results were analyzed using the Image J software.

Reverse transcription-quantitative polymerase chain reaction (RT-qPCR)

Using Trizol (15596026, Thermo), total RNA was isolated from the cultivated cells. UV spectrophotometry was used to detect the concentration and purity of the extracted material. Reverse transcription was performed using a Cwbio kit (CW2569). UltraSYBR Mixture (CW2601, Cwbio) was used for the RT-qPCR reaction. The PCR reaction parameters were as follows: 30 μL system, pre-denaturation at 95°C for 10 min, denaturation at 95°C for 15 s, annealing extension at 60°C for 30 s, and 40 cycles. β-actin served as an internal control. Differences in gene expression levels were computed using the $2^{-\Delta\Delta Ct}$ method. The design of primer sequences was as follows: M-β-actin forward 5'-ACATCCGTAAAGACCTCTATGCC-3', reverse 5'-TACTCCTGCTTGCTGATCCAC-3'; M-ATG5 forward 5'-CACCCCTGAAATGAGTTTTCCA-3', reverse 5'-GGTTGATGGCCCAAAACTGG-3'.

Cell Counting Kit-8 (CCK-8) assay

A 96-well plate was filled with 300 μL of medium with a cell density of 5×10^3 cells per well. The plate was then placed in the incubator to continue to grow. Following treatment, each well received medium contained a 10% CCK8 working solution (AWC0114b, Abiowell). Optical density (OD) at 450 nm was measured using a microplate reader (MB-530, Heales) after incubation for 4 h.

ELISA

The cells and BAL from each group were collected and centrifuged at 1000 ×*g* at 4°C for 15 min. Following aspiration of the supernatant, the levels of IL-6, IL-8, and TNF-α were measured using ELISA kits, following the instructions for IL-6 (CSB-E04639m, Cusabio), IL-8 (EM1592, Wuhan Fine Biotech), and TNF-α (CSB-E04741m, Cusabio).

Immunofluorescence

The slides were fixed in 4% paraformaldehyde for 30 min after washing with PBS 3 times. Following fixation, coverslips were washed for 3-5 min with PBS, permeabilized for 30 min at 37°C with 0.3% Triton X-100, and washed for 3 min with PBS. After blocking for 60 min at 37°C with 5% BSA, the coverslips were washed 3 times with PBS. Primary antibodies against LC3B and METTL3 were added after washing and incubated at 4°C overnight. The coverslips underwent 5-min PBS washes 3 times. Next, 50-100 μL of fluorescently labeled secondary goat anti-rabbit IgG (H+L) antibodies, Alexa Fluor 488 (AWS0005c, 1:200, Abiowell) and goat anti-mouse IgG (H+L), Alexa Fluor 594 (AWS0004c, 1:200, Abiowell) were added and incubated at 37°C for 90 min. Following incubation, the coverslips were washed with PBS three times for 5 min. The cells were rinsed three times with PBS for 5 min each after staining with DAPI working solution (17511, AAT Bioquest) for 10 min at 37°C. A fluorescence microscope (BA410T, Motic) was used to observe the samples.

Methylated RNA immunoprecipitation (MeRIP)-qPCR

The m6A levels of ATG5 in cells were detected using an RNA immunoprecipitation kit (RIP, Sigma). The cells were rinsed twice with PBS, followed by 5-min centrifugation at 200×*g* at room temperature to discard the supernatant. The cell pellet (about 100 μL) was resuspended in 100 μL of RIP lysis buffer and incubated on ice for 5 min before storage at -80°C. Protein A magnetic beads were washed and then resuspended in 100 μL RIP wash buffer. Four μg of m6A antibody (68055-1-Ig, Proteintech) or IgG antibody were added to the corresponding centrifuge tubes and incubated with magnetic beads for 30 min at room temperature. The centrifuge tube with the magnetic beads was placed in a magnetic field to discard the supernatant, and 900 μL of RIP was added. Following lysate thawing, the mixture was centrifuged for 10 min at 4°C at 18756×*g*. The supernatant was then collected and transferred to the pre-prepared centrifuge tube containing magnetic beads. The samples were then incubated overnight at 4°C with rotation. After rinsing with RIP wash buffer, magnetic beads that captured RNA were digested by adding 150 μL Proteinase K (CW2584M, CWbio) work solution (2.4 μg/μL) at 55°C for 30 min. Subsequently, RNA isolation was carried out through TRIzol, followed by RT-qPCR analysis.

RNA stability assay

ATG5 mRNA stability was determined using the previous method [25,26]. Cells that reached 50% confluence were treated with actinomycin D (5 μg/mL) for 0, 2, 6, 12, and 24 h. Following this step, the cells were harvested, and ATG5 mRNA levels were measured using RT-qPCR.

Statistical analysis

Statistical analysis was performed using GraphPad Prism 8.0.1 software, and all data were presented as the mean±standard deviation (SD). For samples that followed a normal distribution, comparisons between two groups were performed using the t-test, comparisons among multiple groups were conducted using one-way and two-way analysis of variance (ANOVA) tests, and post hoc multiple comparisons were performed using Tukey's multiple comparison tests. A significance level of $P<0.05$ was considered statistically significant. Each experiment was repeated 3 times, and each group was set up with at least 3 independent samples.

RESULTS

METTL3 was upregulated in the lung tissue of COPD mice

To elucidate the function of METTL3 in the progression of COPD, we investigated its correlation with autophagy and inflammatory factors. The H&E staining results (Fig. 1A) revealed that compared to the control group, the airway wall of mice in the COPD group was thicker, the airway structure was disrupted, and fibrotic changes and inflammatory cell infiltration were observed. The lung injury score, mean alveolar septal thickness, and mean linear intercept of alveoli of mice in the COPD group were significantly higher than in the control group. The mean alveolar number was lower than in the control group (Fig. 1B). Masson staining indicated that collagen deposition in the lung tissue of COPD mice was higher than that in the control group (Fig. 1C). Western blot analysis revealed an apparent increase in the levels of METTL3, LC3B, ATG5, and p-p65/p65 in lung tissues of COPD mice; the levels of p62 were significantly lower than in the control group (Fig. 1D-1E). ELISA results showed the levels of IL-6, IL-8, and TNF-α in the BAL fluid of lung tissues were higher than those in the control group (Fig. 1F-1H). N-cadherin, α-SMA, and Tn-C protein levels in lung tissues were higher in the COPD group than in the control group. In contrast, the E-cadherin level was significantly decreased (Fig. 1I). The expression of METTL3 was positively correlated with LC3B, ATG5, IL-6, IL-8, and TNF-α, according to Pearson's correlation analysis (Fig. 1J-1K). These findings showed that METTL3 expression was increased in the lung tissues of COPD mice, and there was a positive correlation between METTL3 expression and LC3B, ATG5, IL-6, IL-8, and TNF-α in COPD lung tissues.

METTL3 reduction was followed by lower CSE-mediated macrophage autophagy

To investigate the effect of METTL3 on CSE-mediated macrophage autophagy, we measured the autophagy

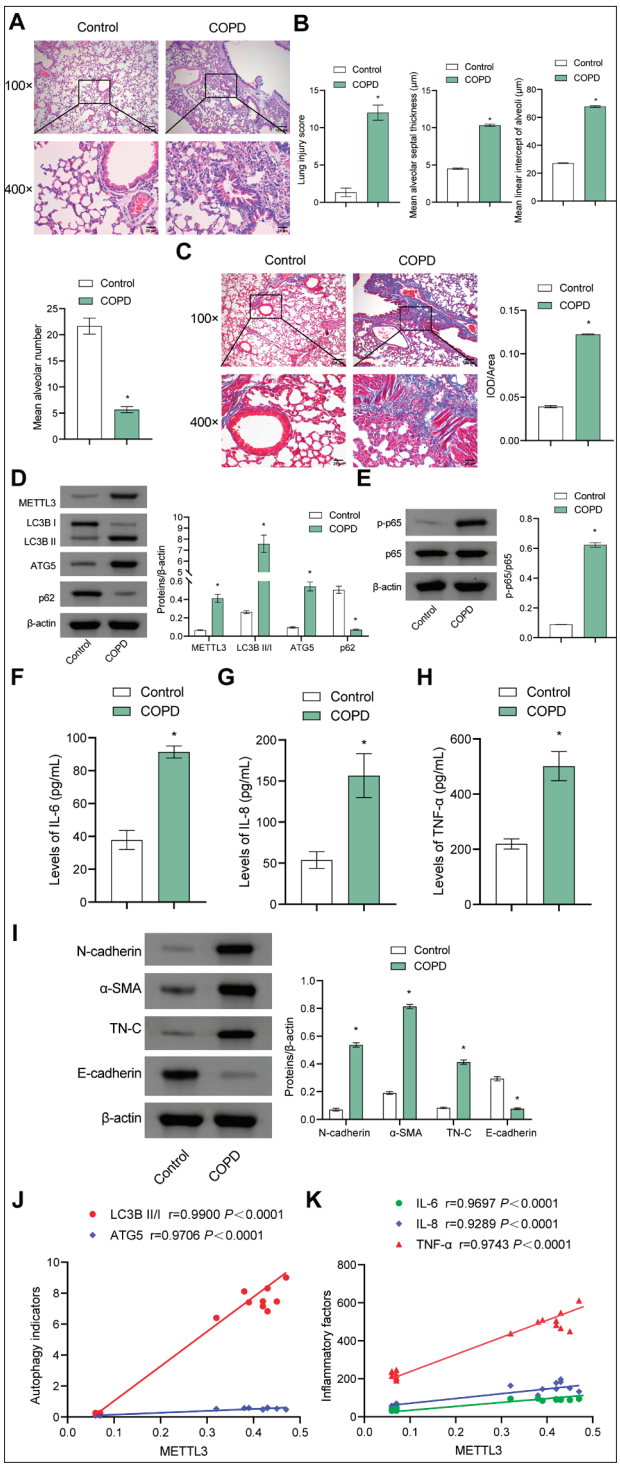

Fig. 1. METTL3 was upregulated in the lung tissue of COPD mice. **A** – H&E staining images of lung tissue in mice. **A, B** – The result of lung injury score, mean alveolar septal thickness, mean linear intercept of alveoli, and mean alveolar number. **C** – Masson staining of lung tissue in mice. **D, E** – The levels of METTL3, LC3B, ATG5, p62, and p-p65/p65 detected by Western blotting. **F, G, H** – IL-6, IL-8, and TNF-α levels detected by ELISA. **I** – The E-cadherin, N-cadherin, α-SMA, and Tn-C levels estimated by Western blotting. **J, K** – Pearson correlation analysis of METTL3 with LC3B, ATG5, IL-6, IL-8 and TNF-α. *P<0.05 vs. the control.

level in macrophages after METTL3 knockdown. Results from the CCK-8 assay showed that at 24 h and 48 h, the cell viability of RAW264.7 cells treated with 1%, 2.5%, 5%, and 10% CSE was lower than that of the 0% CSE group, with the lowest cell viability observed in the 10% CSE group (Fig. 2A). The 10% CSE group was selected for subsequent studies. As shown in Fig. 2B, the levels of METTL3 in the si-METTL3#1, si-METTL3#2, and si-METTL3#3 groups were significantly lower than in the si-NC group, with the lowest level observed in the si-METTL3#1 group. We selected si-METTL3#1 for further studies.

As shown in Fig. 2C and D, the CSE group displayed higher METTL3, LC3B II/I, and ATG5 levels than the control group, but the p62 level was lower. The CSE+si-METTL3 group exhibited significantly decreased levels in METTL3, LC3B II/I, and ATG5 compared to the CSE+si-NC group, with an increase in p62. The addition of rapamycin led to significant rises in METTL3, LC3B II/I, and ATG5 levels and a decrease in p62. The CSE group's LC3B levels were higher than those in the control group. LC3B levels in the CSE+si-METTL3 group were significantly lower than in the CSE+si-NC group. After rapamycin intervention, there was an increase in LC3B levels (Fig. 2E, Supplementary Fig. S1). As shown in Fig. 2F, the levels of p-p65/p65 in the CSE group were significantly higher than in the control group, while the levels of p-p65/p65 in the CSE+si-METTL3 group were lower than in the CSE+si-NC group. Rapamycin reversed the effects of METTL3 knockdown. These results showed that reduced levels of METTL3 were accompanied by decreased levels of autophagy parameters, indicating that METTL3 may have a promoting effect on CSE-mediated macrophage autophagy.

METTL3 promoted CSE-mediated macrophage autophagy through m6A-dependent regulation of ATG5

To investigate whether METTL3 regulates ATG5 through m6A-dependent mechanisms in COPD, we measured the m6A and mRNA levels of ATG5 after inhibiting METTL3. The si-METTL3 group showed a decrease in both m6A and mRNA levels of ATG5 compared to the si-NC group (Fig. 3A and B). These findings suggest that METTL3 regulates the expression of ATG5. There was no discernible difference

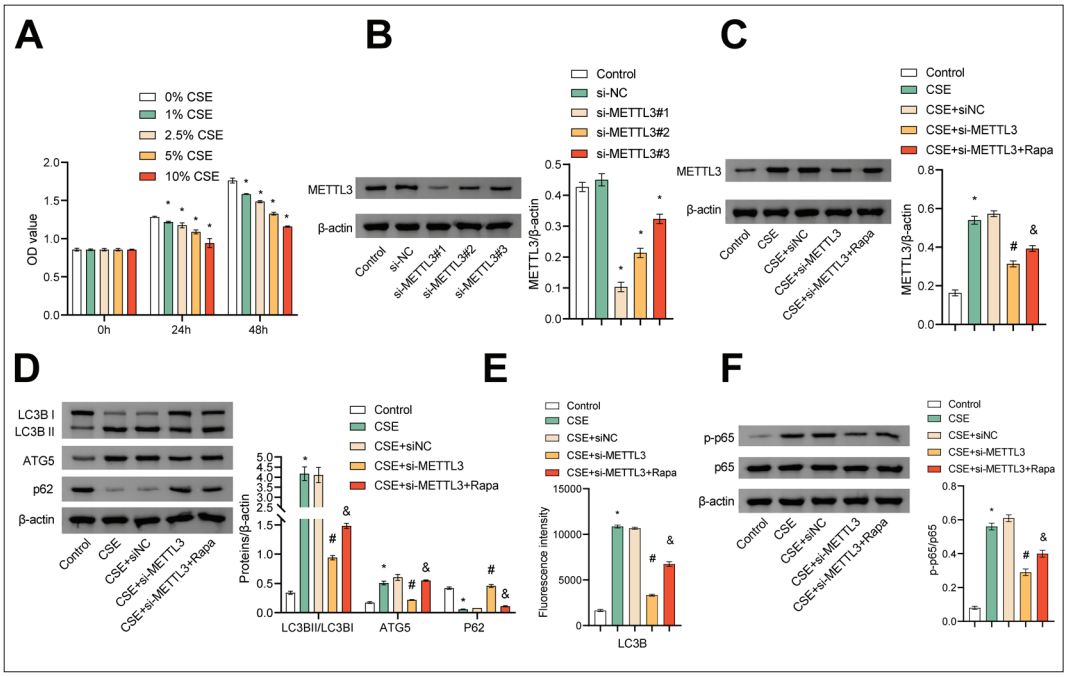

Fig. 2. METTL3 enhanced CSE-mediated macrophage autophagy. **A** – The CCK-8 test used to determine the viability of RAW264.7 cells. **B, C** – The levels of METTL3 detected by Western blotting. **D** – The levels of LC3B, ATG5, and p62 measured by Western blotting. **E** – Immunofluorescence staining of LC3B. **F** – The levels of p-p65/p65 assessed by Western blotting. *P<0.05 vs. the control, #P<0.05 vs. CSE+si-NC, &P<0.05 vs. CSE+si-METTL3.

between the si-NC group and the control group in the ATG5 mRNA stability assay; after knocking down METTL3, the stability of ATG5 mRNA decreased (Fig. 3C). To further investigate the impact of the METTL3-ATG5 axis on macrophage autophagy, we measured autophagy levels in macrophages following METTL3 knockdown and ATG5 overexpression. ATG5 levels did not differ significantly between the oe-NC and control groups. In contrast, the oe-ATG5 group exhibited higher ATG5 levels than the oe-NC group (Fig. 3D), indicating that oe-ATG5 was successfully transfected. Fig. 3E shows that METTL3, LC3B II/I, and ATG5 levels in the CSE group were considerably higher than in the control group, whereas the p62 level was lower. Knocking down METTL3 caused an apparent decline in METTL3, LC3B II/I, and ATG5 levels and an increase in p62 levels. ATG5 overexpression caused an increase in METTL3, LC3B II/I, and ATG5 and a decline in p62. Immunofluorescence results showed higher levels of METTL3 and LC3B in the CSE group than in the control group.

The knockdown of METTL3 led to a decrease in METTL3 and LC3B. Transfection with ATG5 overexpression led to a significant increase in the levels of METTL3 and LC3B (Fig. 3F, Supplementary Fig. S2). As shown in Fig. 3G, the p-p65/p65 level in the CSE group was higher than in the control group. Knockdown of METTL3 led to an essential decrease in p-p65/p65, whereas transfection of ATG5 overexpression significantly increased p-p65/p65. These results indicate that METTL3 regulates ATG5 expression through m6A modification promoting CSE-mediated macrophage autophagy. Also, ATG5 overexpression led to a significant increase in METTL3 (Fig. 3E).

Inhibition of METTL3-ATG5-mediated macrophage autophagy alleviated the bronchial epithelial cell inflammatory response and airway remodeling

To study whether METTL3-ATG5-mediated macrophage autophagy could affect bronchial epithelial cell inflammation and airway remodeling, we co-cultured mouse bronchial epithelial cells with macrophages and assessed the relevant indicators of these processes in bronchial epithelial cells. As shown in Fig. 4A, p-p65/p65 in the CSE group was higher than in the control group. However, METTL3 knockdown led to a decline

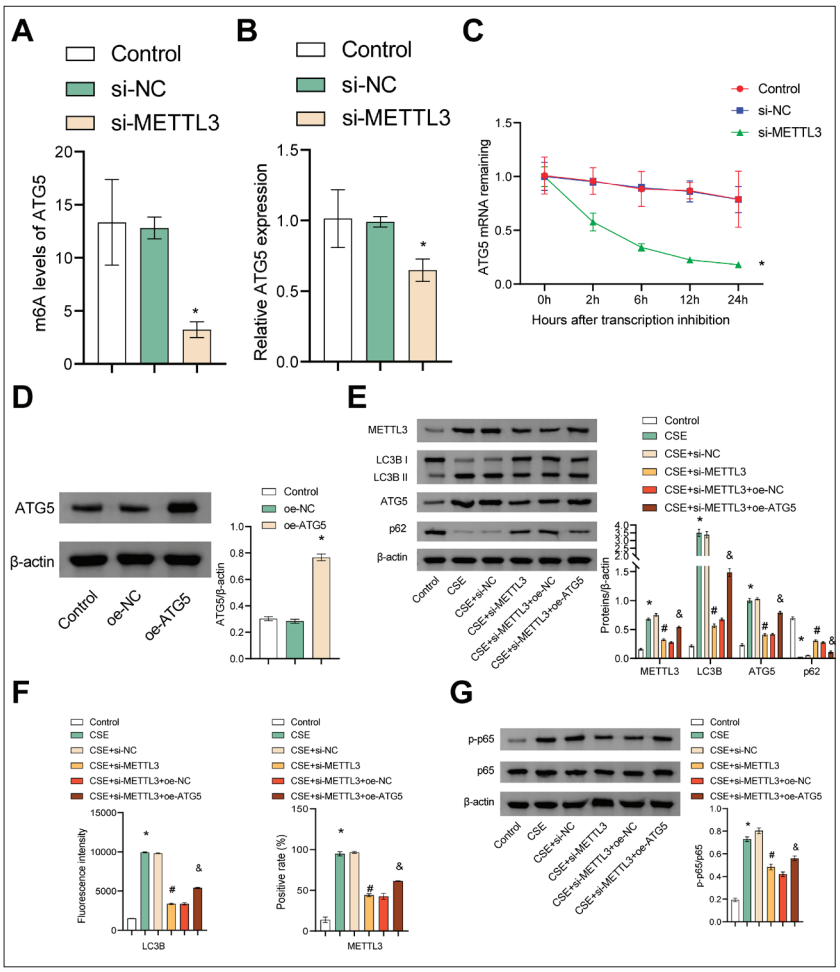

Fig. 3. METTL3 promoted CSE-mediated macrophage autophagy through m6A-dependent regulation of ATG5. **A** – MeRIP-qPCR for m6A levels of ATG5 in RAW264.7 cells. **B** – ATG5 levels assessed by RT-qPCR. **C** – ATG5 mRNA stabilization assay. **D** - The levels of ATG5 measured by Western blotting. **E** – LC3B, ATG5, and p62 levels measured by Western blotting. **F** – Immunofluorescence staining of LC3B and METTL3. **G** – p-p65/p65 levels measured by Western blotting. *P<0.05 vs. the control, #P<0.05 vs. CSE+si-NC, &P<0.05 vs. CSE+si-METTL3+oe-NC.

in p-p65/p65 levels. The level of p-p65/p65 was significantly increased with the addition of rapamycin. ELISA results showed that the CSE group had considerably higher IL-6, IL-8, and TNF-α levels than the control group. IL-6, IL-8, and TNF-α levels decreased when METTL3 was knocked down but significantly increased when rapamycin was added (Fig. 4B, C, and D). Western blotting results revealed that the levels of N-cadherin, α-SMA, and Tn-C in the CSE group were higher than in the control group, while the E-cadherin level was significantly decreased. Knockdown of METTL3 led to a decline in N-cadherin, α-SMA, and Tn-C levels, and a significant increase in E-cadherin. Rapamycin addition led to increases in N-cadherin, α-SMA, and Tn-C levels and a decline in E-cadherin (Fig. 4E). These results show that inhibiting METTL3-ATG5-mediated macrophage autophagy reduces bronchial epithelial cell inflammation and airway remodeling.

DISCUSSION

METTL3 plays an essential role in multiple biological processes [27]. Studies have revealed increased expression of METTL3 in COPD, which was significantly correlated with genes enriched in signaling pathways and biological processes that promote the progression of COPD [18,28]. In this study, we discovered that METTL3 could influence the progression of COPD by regulating macrophage-damaging autophagy mediated by ATG5.

Previous studies have shown that cigarette smoke exposure can cause abnormal inflammatory responses in the airways and alveoli [29]. Long-term exposure to cigarette smoke is also the main cause of COPD [30,31]. The occurrence and progression of COPD are closely associated with CSE-induced dysregulation of lung cell autophagy [8]. In this study, the lung tissues of COPD mice were infiltrated by inflammatory cells, and the airways were disrupted. This result was consistent with previous findings [32]. CSE leads to increased macrophage-damaging autophagy, with an increase in ATG5 [7]. Our results showed that cigarette smoke-induced COPD mouse lung tissue inflammation and airway remodeling increased concurrently with an increase in autophagy mediated by ATG5. CSE has been reported to increase LC3B-II expression and induce macrophage-damaging autophagy [33]. Macrophages play a central role in coordinating inflammation, emphysema formation, and lung parenchymal destruction in COPD patients [34]. An increase in macrophage counts has been reported in the sputum, BAL fluid,

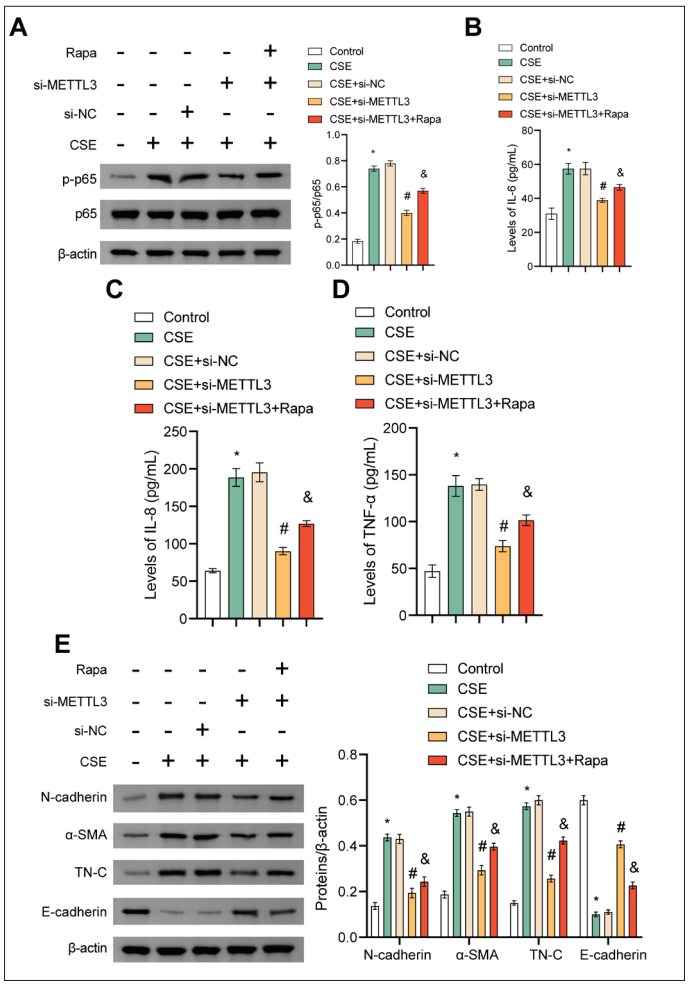

Fig. 4. Inflammatory response markers and airway remodeling were alleviated in mouse bronchial epithelial cells co-cultured with macrophages inhibiting the METTL3-ATG5 axis. **A** – The levels of p-p65/p65 in mouse bronchial epithelial cells were measured by Western blotting. **B, C, D** – The levels of IL-6, IL-8, and TNF-α in the mouse bronchial epithelial cell supernatant detected by ELISA. **E** – The levels of E-cadherin, N-cadherin, α-SMA, and Tn-C in mouse bronchial epithelial cells estimated by Western blotting. *P<0.05 vs. the control, #P<0.05 vs. CSE+si-NC, &P<0.05 vs. CSE+si-METTL3.

lung parenchyma, and airways of COPD patients [35]. Based on this, we speculated that CSE stimulation enhances ATG5-mediated macrophage-damaging autophagy, exacerbated inflammation, and airway remodeling in COPD mice.

The potential role of m6A modifications in COPD is a hot topic [24]. In smoking-induced COPD patients and cell models of COPD, the expression of METTL3 was significantly increased [18]. METTL3 has been shown to promote autophagy by stabilizing ATG5 mRNA in osteosarcoma [36]. Increased METTL3 expression upregulates NF-κB and other inflammatory factors in microglial cells [37]. Herein we report that METTL3 expression was elevated in the lung tissues of COPD mice and positively correlated with ATG5 and inflammation markers. Therefore, METTL3 may regulate macrophage-damaging autophagy mediated by ATG5, affecting COPD inflammation and airway remodeling. Furthermore, the present study demonstrated that knocking down METTL3 alleviated the expression of the markers of inflammation and fibrosis in mouse bronchial epithelial cells co-cultured with RAW264.7 cells treated with CSE. The autophagy inducer rapamycin reversed the effects of METTL3 knockdown. Considering the above, we propose that METTL3 exacerbates bronchial epithelial cell inflammation and airway remodeling by enhancing CSE-induced macrophage-damaging autophagy.

Studies have shown that the level of m6A modification is abnormally expressed in the lung tissues of COPD patients [38]. METTL3 is the core catalytic enzyme of m6A and plays a critical role in m6A modification [39]. ATG5 is a key gene in the autophagy process, along with autophagy-related proteins such as ATG12/16L and LC3, which collectively participate in the extension of autophagic vesicles and drive the autophagic process [40]. In our study, we found that METTL3 enhanced the mRNA stability of ATG5 by increasing the m6A level of ATG5, and that ATG5 overexpression increased the autophagy level of macrophages. This result indicated that METTL3 promoted ATG5 mRNA transcription in an m6A-dependent manner and that ATG5 was associated with impaired autophagy in COPD macrophages. METTL3 upregulated the expression of ATG5 through m6A modification, thereby promoting macrophage-damaging autophagy.

The crosstalk between autophagy and the RNA methylation/demethylation pathway is complex. FTO, an m6A demethylase, could elevate ATG5 expression via YTHDF2 in mouse pre-adipose cells; the decrease of ATG5 conversely leads to a reduction in FTO in melanoma [41]. Let-7g is a microRNA targeting 3'-UTR of METTL3 and promoting its expression. In breast

cancer, hepatitis B, virus X-interacting protein (HBXIP) protein enhances METTL3 expression by inhibiting let-7g, while METTL3 could promote HBXIP expression by upregulating the m6A modification levels of HBXIP, forming a positive feedback loop [42]. In the present study, we observed that ATG5 was diminished after METTL3 knockdown, while overexpressed ATG5 resulted in the elevation of METTL3. These results indicate the presence of positive feedback mechanisms involving other molecules in the regulation of the METTL3-ATG5 axis. Future studies utilizing high-throughput biological experimental techniques may uncover these mechanisms and offer new insights for treating COPD.

Our study further explored the impact of down-regulating METTL3 expression in mouse bronchial epithelial cells co-cultured with macrophages. The results showed that inhibiting the METTL3-ATG5 axis reduced the destructive autophagy of macrophages, which may alleviate the bronchial epithelial cell inflammatory response and reduce airway remodeling. However, we only investigated the impact of METTL3-ATG5-mediated macrophage-damaging autophagy on mouse bronchial epithelial cells. Given the differences between species, we intend to further validate the findings of this study in a clinical setting, and in human cells.

In conclusion, our study demonstrates that inhibiting METTL3 expression can mitigate ATG5-mediated harmful autophagy in macrophages, leading to a reduction in bronchial epithelial inflammation and airway remodeling associated with COPD. This research introduces novel concepts for potential interventions and treatments for the disease.

Funding: This study was sponsored by the Science Foundation of Hunan Aerospace Hospital, 2023YJ03.

Author contributions: Data curation: ZX, XZ; formal analysis, and visualization: GC, ZX, XZ; writing-original draft: GC; conceptualization, project administration, and writing and editing: HL. All authors reviewed the results and approved the final version of the manuscript.

Conflict of interest disclosure: The authors do not have any conflict of interest to declare.

Data availability: The dataset underlying the reported findings is available here: https://www.serbiosoc.org.rs/NewUploads/Uploads/Chen%20et%20al_Dataset.pdf

REFERENCES

1. Gordon A, Young M, Bihler E, Cheema T. COPD Maintenance Pharmacotherapy. Crit Care Nurs Q. 2021;44(1):19-25. https://doi.org/10.1097/cnq.0000000000000336
2. Hogea SP, Tudorache E, Fildan AP, Fira-Mladinescu O, Marc M, Oancea C. Risk factors of chronic obstructive pulmonary disease exacerbations. Clin Respir J. 2020;14(3):183-97. https://doi.org/10.1111/crj.13129
3. Xie W, Zheng W, Liu M, Qin Q, Zhao Y, Cheng Z, Guo F. BRF1 ameliorates LPS-induced inflammation through autophagy crosstalking with MAPK/ERK signaling. Genes Dis. 2018;5(3):226-34. https://doi.org/10.1016/j.gendis.2018.04.004
4. Bodas M, Patel N, Silverberg D, Walworth K, Vij N. Master Autophagy Regulator Transcription Factor EB Regulates Cigarette Smoke-Induced Autophagy Impairment and Chronic Obstructive Pulmonary Disease-Emphysema Pathogenesis. Antioxid Redox Signal. 2017;27(3):150-67. https://doi.org/10.1089/ars.2016.6842
5. Wu Y, Li D, Wang Y, Chen K, Yang K, Huang X, Zhang Y, Wu M. Pseudomonas aeruginosa promotes autophagy to suppress macrophage-mediated bacterial eradication. Int Immunopharmacol. 2016;38:214-22. https://doi.org/10.1016/j.intimp.2016.04.044
6. Wu H, Ma H, Wang L, Zhang H, Lu L, Xiao T, Cheng C, Wang P, Yang Y, Wu M, Wang S, Zhang J, Liu Q. Regulation of lung epithelial cell senescence in smoking-induced COPD/emphysema by microR-125a-5p via Sp1 mediation of SIRT1/HIF-1a. Int J Biol Sci. 2022;18(2):661-74. https://doi.org/10.7150/ijbs.65861
7. Kono Y, Colley T, To M, Papaioannou AI, Mercado N, Baker JR, To Y, Abe S, Haruki K, Ito K, Barnes PJ. Cigarette smoke-induced impairment of autophagy in macrophages increases galectin-8 and inflammation. Sci Rep. 2021;11(1):335. https://doi.org/10.1038/s41598-020-79848-0
8. Xu SW, Zhang YJ, Liu WM, Zhang XF, Wang Y, Xiang SY, Su JC, Liu ZB. Cigarette smoke extract-induced inflammatory response via inhibition of the TFEB-mediated autophagy in NR8383 cells. Exp Lung Res. 2023;49(1):39-48. https://doi.org/10.1080/01902148.2022.2164674
9. Wang L, Yu Q, Xiao J, Chen Q, Fang M, Zhao H. Cigarette Smoke Extract-Treated Mouse Airway Epithelial Cells-Derived Exosomal LncRNA MEG3 Promotes M1 Macrophage Polarization and Pyroptosis in Chronic Obstructive Pulmonary Disease by Upregulating TREM-1 via m(6)A Methylation. Immune Netw. 2024;24(2):e3. https://doi.org/10.4110/in.2024.24.e3
10. Wu YF, Li ZY, Dong LL, Li WJ, Wu YP, Wang J, Chen HP, Liu HW, Li M, Jin CL, Huang HQ, Ying SM, Li W, Shen HH, Chen ZH. Inactivation of MTOR promotes autophagy-mediated epithelial injury in particulate matter-induced airway inflammation. Autophagy. 2020;16(3):435-50. https://doi.org/10.1080/15548627.2019.1628536
11. Zheng W, Xie W, Yin D, Luo R, Liu M, Guo F. ATG5 and ATG7 induced autophagy interplays with UPR via PERK signaling. Cell Commun Signal. 2019;17(1):42. https://doi.org/10.1186/s12964-019-0353-3
12. Zhou L, Haiyilati A, Li J, Li X, Gao L, Cao H, Wang Y, Zheng SJ. Gga-miR-30c-5p Suppresses Avian Reovirus (ARV) Replica-

tion by Inhibition of ARV-Induced Autophagy via Targeting ATG5. J Virol. 2022;96(14):e0075922. https://doi.org/10.1128/jvi.00759-22
13. Qiang L, Yang S, Cui YH, He YY. Keratinocyte autophagy enables the activation of keratinocytes and fibroblastsand facilitates wound healing. Autophagy. 2021;17(9):2128-43. https://doi.org/10.1080/15548627.2020.1816342
14. Li J, Yang X, Qi Z, Sang Y, Liu Y, Xu B, Liu W, Xu Z, Deng Y. The role of mRNA m(6)A methylation in the nervous system. Cell Biosci. 2019;9:66. https://doi.org/10.1186/s13578-019-0330-y
15. Shen C, Xuan B, Yan T, Ma Y, Xu P, Tian X, Zhang X, Cao Y, Ma D, Zhu X, Zhang Y, Fang JY, Chen H, Hong J. m(6)A-dependent glycolysis enhances colorectal cancer progression. Mol Cancer. 2020;19(1):72. https://doi.org/10.1186/s12943-020-01190-w
16. Xia H, Wu Y, Zhao J, Cheng C, Lin J, Yang Y, Lu L, Xiang Q, Bian T, Liu Q. N6-Methyladenosine-modified circSAV1 triggers ferroptosis in COPD through recruiting YTHDF1 to facilitate the translation of IREB2. Cell Death Differ. 2023;30(5):1293-304. https://doi.org/10.1038/s41418-023-01138-9
17. Chai RC, Chang YZ, Chang X, Pang B, An SY, Zhang KN, Chang YH, Jiang T, Wang YZ. YTHDF2 facilitates UBXN1 mRNA decay by recognizing METTL3-mediated m(6)A modification to activate NF-κB and promote the malignant progression of glioma. J Hematol Oncol. 2021;14(1):109. https://doi.org/10.1186/s13045-021-01124-z
18. Zhang Y, Wang L, Yan F, Yang M, Gao H, Zeng Y. Mettl3 Mediated m6A Methylation Involved in Epithelial-Mesenchymal Transition by Targeting SOCS3/STAT3/SNAI1 in Cigarette Smoking-Induced COPD. Int J Chron Obstruct Pulmon Dis. 2023;18:1007-17. https://doi.org/10.2147/COPD.S398289
19. Chen H, Xiang Y, Yin Y, Peng J, Peng D, Li D, Kitazawa R, Tang Y, Yang J. The m6A methyltransferase METTL3 regulates autophagy and sensitivity to cisplatin by targeting ATG5 in seminoma. Transl Androl Urol. 2021;10(4):1711-22. https://doi.org/10.21037/tau-20-1411
20. Wang L, Chen Q, Yu Q, Xiao J, Zhao H. Cigarette smoke extract-treated airway epithelial cells-derived exosomes promote M1 macrophage polarization in chronic obstructive pulmonary disease. Int Immunopharmacol. 2021;96:107700. https://doi.org/10.1016/j.intimp.2021.107700
21. He S, Tian R, Zhang X, Yao Q, Chen Q, Liu B, Liao L, Gong Y, Yang H, Wang D. PPARγ inhibits small airway remodeling through mediating the polarization homeostasis of alveolar macrophages in COPD. Clin Immunol. 2023;250:109293. https://doi.org/10.1016/j.clim.2023.109293
22. Liu H, Wang XX, Chen P. Angiopoietin-like 4 knockdown attenuates cigarette smoke extract-induced oxidative stress and apoptosis in lung bronchial epithelial cells by inhibiting NADPH oxidase. Allergol Immunopathol (Madr). 2022;50(5):47-56. https://doi.org/10.15586/aei.v50i5.637
23. Chen H, Yu Y, Yang M, Huang H, Ma S, Hu J, Xi Z, Guo H, Yao G, Yang L, Huang X, Zhang F, Tan G, Wu H, Zheng W, Li L. YTHDF1 promotes breast cancer progression by facilitating FOXM1 translation in an m6A-dependent manner. Cell Biosci. 2022;12(1):19. https://doi.org/10.1186/s13578-022-00759-w
24. Xie B, Dai Z, Jiang C, Gao X, Yang S, Peng M, Chen Q, Chen X. ZC3H13 promotes ITGA6 m(6)A modification for chronic obstructive pulmonary disease progression. Cell Signal. 2024;120:111190. https://doi.org/10.1016/j.cellsig.2024.111190
25. Xie F, Huang C, Liu F, Zhang H, Xiao X, Sun J, Zhang X, Jiang G. CircPTPRA blocks the recognition of RNA N(6)-methyladenosine through interacting with IGF2BP1 to suppress bladder cancer progression. Mol Cancer. 2021;20(1):68. https://doi.org/10.1186/s12943-021-01359-x
26. Wang F, Bai J, Zhang X, Wang D, Zhang X, Xue J, Chen H, Wang S, Chi B, Li J, Ma X. METTL3/YTHDF2 m6A axis mediates the progression of diabetic nephropathy through epigenetically suppressing PINK1 and mitophagy. J Diabetes Investig. 2024;15(3):288-99. https://doi.org/10.1111/jdi.14113
27. Chen M, Wei L, Law CT, Tsang FH, Shen J, Cheng CL, Tsang LH, Ho DW, Chiu DK, Lee JM, Wong CC, Ng IO, Wong CM. RNA N6-methyladenosine methyltransferase-like 3 promotes liver cancer progression through YTHDF2-dependent posttranscriptional silencing of SOCS2. Hepatology. 2018;67(6):2254-70. https://doi.org/10.1002/hep.29683
28. Huang X, Lv D, Yang X, Li M, Zhang H. m6A RNA methylation regulators could contribute to the occurrence of chronic obstructive pulmonary disease. J Cell Mol Med. 2020;24(21):12706-15. https://doi.org/10.1111/jcmm.15848
29. Yoshida M, Minagawa S, Araya J, Sakamoto T, Hara H, Tsubouchi K, Hosaka Y, Ichikawa A, Saito N, Kadota T, Sato N, Kurita Y, Kobayashi K, Ito S, Utsumi H, Wakui H, Numata T, Kaneko Y, Mori S, Asano H, Yamashita M, Odaka M, Morikawa T, Nakayama K, Iwamoto T, Imai H, Kuwano K. Involvement of cigarette smoke-induced epithelial cell ferroptosis in COPD pathogenesis. Nat Commun. 2019;10(1):3145. https://doi.org/10.1038/s41467-019-10991-7
30. Li C, Chen F, Lin L, Li J, Zheng Y, Chen Q. CSE triggers ferroptosis via SIRT4-mediated GNPAT deacetylation in the pathogenesis of COPD. Respir Res. 2023;24(1):301. https://doi.org/10.1186/s12931-023-02613-0
31. Li SH, Li QP, Chen WJ, Zhong YY, Sun J, Wu JF, Cao YX, Dong JC. Psoralen attenuates cigarette smoke extract-induced inflammation by modulating CD8(+) T lymphocyte recruitment and chemokines via the JAK2/STAT1 signaling pathway. Heliyon. 2024;10(12):e32351. https://doi.org/10.1016/j.heliyon.2024.e32351
32. Eom JE, Kim GD, Kim YI, Lim KM, Song JH, Kim Y, Song HJ, Shin DU, Lim EY, Kim HJ, Kim SH, Lee DS, Lee SY, Shin HS. Bulb of *Lilium longiflorum* Thunb Extract Fermented with Lactobacillus acidophilus Reduces Inflammation in a Chronic Obstructive Pulmonary Disease Model. J Microbiol Biotechnol. 2023;33(5):634-43. https://doi.org/10.4014/jmb.2301.01022
33. Pei C, Wang X, Lin Y, Fang L, Meng S. Inhibition of Galectin-3 Alleviates Cigarette Smoke Extract-Induced Autophagy and Dysfunction in Endothelial Progenitor Cells. Oxid Med Cell Longev. 2019;2019:7252943. https://doi.org/10.1155/2019/7252943
34. Zhang J, Zhao Y, Hou T, Zeng H, Kalambhe D, Wang B, Shen X, Huang Y. Macrophage-based nanotherapeutic strategies in ulcerative colitis. J Control Release. 2020;320:363-80. https://doi.org/10.1016/j.jconrel.2020.01.047
35. Liu J, Zhang Z, Yang Y, Di T, Wu Y, Bian T. NCOA4-Mediated Ferroptosis in Bronchial Epithelial Cells Promotes Macrophage M2 Polarization in COPD Emphysema. Int J Chron Obstruct Pulmon Dis. 2022;17:667-81. https://doi.org/10.2147/COPD.S354896

36. Wang C, Meng Y, Zhao J, Ma J, Zhao Y, Gao R, Liu W, Zhou X. Deubiquitinase USP13 regulates glycolytic reprogramming and progression in osteosarcoma by stabilizing METTL3/m(6)A/ATG5 axis. Int J Biol Sci. 2023;19(7):2289-303. https://doi.org/10.7150/ijbs.82081
37. Wen L, Sun W, Xia D, Wang Y, Li J, Yang S. The m6A methyltransferase METTL3 promotes LPS-induced microglia inflammation through TRAF6/NF-κB pathway. Neuroreport. 2022;33(6):243-51. https://doi.org/10.1097/wnr.0000000000001550
38. Hu T, Xu L, Jiang M, Zhang F, Li Q, Li Z, Wu C, Ding J, Li F, Wang J. N6-methyladenosine-methylomic landscape of lung tissues of mice with chronic obstructive pulmonary disease. Front Immunol. 2023;14:1137195. https://doi.org/10.3389/fimmu.2023.1137195
39. Yankova E, Blackaby W, Albertella M, Rak J, De Braekeleer E, Tsagkogeorga G, Pilka ES, Aspris D, Leggate D, Hendrick AG, Webster NA, Andrews B, Fosbeary R, Guest P, Irigoyen N, Eleftheriou M, Gozdecka M, Dias JML, Bannister AJ, Vick B, Jeremias I, Vassiliou GS, Rausch O, Tzelepis K, Kouzarides T. Small-molecule inhibition of METTL3 as a strategy against myeloid leukaemia. Nature. 2021;593(7860):597-601. https://doi.org/10.1038/s41586-021-03536-w
40. Kharaziha P, Panaretakis T. Dynamics of Atg5-Atg12-Atg16L1 Aggregation and Deaggregation. Methods Enzymol. 2017;587:247-55. https://doi.org/10.1016/bs.mie.2016.09.059
41. Ma Q, Long S, Gan Z, Tettamanti G, Li K, Tian L. Transcriptional and Post-Transcriptional Regulation of Autophagy. Cells. 2022;11(3). https://doi.org/10.3390/cells11030441
42. Cai X, Wang X, Cao C, Gao Y, Zhang S, Yang Z, Liu Y, Zhang X, Zhang W, Ye L. HBXIP-elevated methyltransferase METTL3 promotes the progression of breast cancer via inhibiting tumor suppressor let-7g. Cancer Lett. 2018;415:11-9. https://doi.org/10.1016/j.canlet.2017.11.018

SUPPLEMENTARY MATERIAL

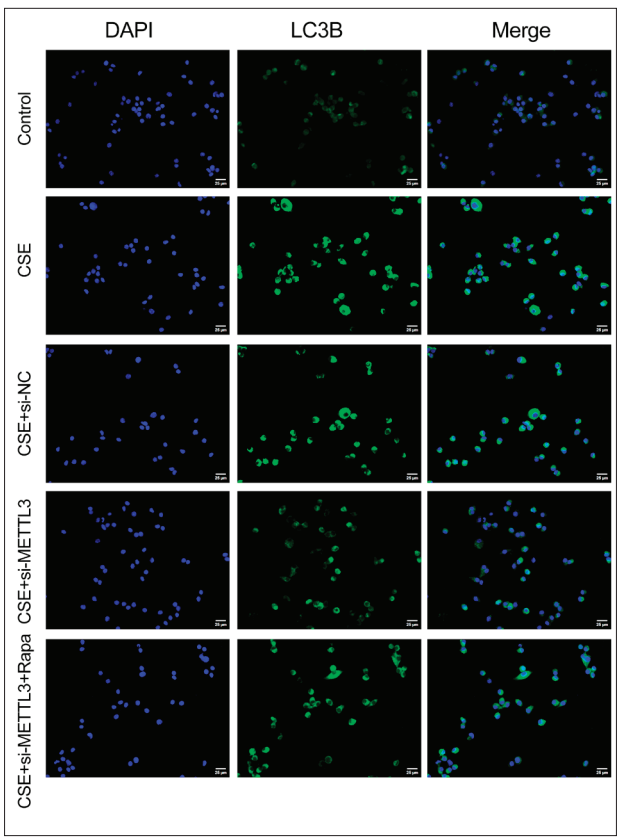

Supplementary Fig. S1. LC3 immunofluorescence staining of Fig. 2E.

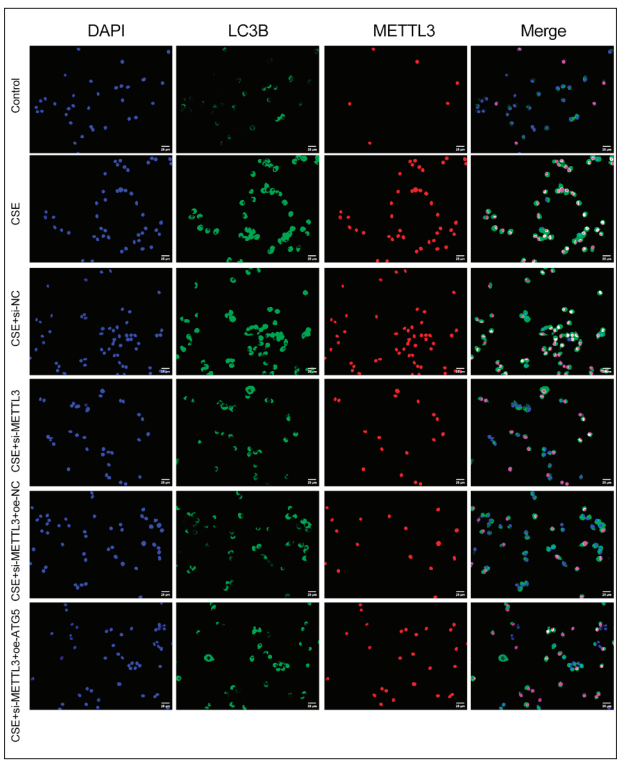

Supplementary Fig. S2. LC3 and METTL3 immunofluorescence staining of Fig. 3F.